Double stall

Bak, Christian; Aagaard Madsen , Helge; Fuglsang, Peter; Rasmussen, Flemming

Publication date:
1998

Document Version
Publisher's PDF, also known as Version of record

Risø-R-1043(EN)

Double Stall

Christian Bak, Helge Aagaard Madsen, Peter Fuglsang, Flemming Rasmussen

Risø National Laboratory, Roskilde
June 1998

Abstract The double stall phenomenon for airfoil flows is characterised by at least two distinct stall levels to identical inflow conditions. In this work, a likely explanation of double stall was found. Observations on full-scale rotors, in wind tunnel experiments and in computational fluid dynamic (CFD) calculations could show at least two different distinct lift levels to identical inflow conditions in stall. The CFD calculations revealed a generation of a little laminar separation bubble at the leading edge of the airfoil for incidences near maximum lift. The bursting of this bubble could explain the sudden shift in lift levels. This investigation indicated that bursting would appear if the maximum position of the free transition point was close to the minimum position of the transition point causing leading-edge stall. Thus, the investigation indicated that double stall could be predicted from CFD calculations and that double stall therefore could be avoided in design of new airfoils.

The present work was funded partly by the Danish Energy Agency under the contract: ENS 1363/97-0002

ISBN 87-550-2379-7
ISBN 87-550-2417-3 (Internet)
ISSN 0106-2840

Information Service Department, Risø, 1998

Contents

List of symbols

A	Blade segment area
c	Chord length
$C_L=C_N \cdot cos(\alpha)+C_T \cdot sin(\alpha)$	Lift coefficient
$C_{L,max}$	Maximum lift coefficient
$C_N=F_N/(q \cdot A)$	Normal force coefficient
$C_p=(p-p_0)/q$	Pressure coefficient
$C_T=F_T/(q \cdot A)$	Tangential force coefficient
F_N	Force normal to chordwise direction (positive towards the upper surface)
F_T	Force in chordwise direction (positive against flow direction)
h	Height of laminar separation bubble
l	Length of laminar separation bubble
$q=\rho \cdot U^2/2$	Dynamic pressure
p	Pressure on the airfoil surface
p_0	Pressure in the far field
R	Rotor radius
$Re = U \cdot c/\nu$	Reynolds number based on airfoil chord
U	Free stream velocity
x, y	Cartesian co-ordinates. x in chordwise direction and y normal to the chord. Origo at the leading edge.
x_{tr}	Transition point location
$x_{tr,stall}$	Min. x_{tr} causing leading-edge stall assuming fixed transition
$x_{tr,max}$	Max. x_{tr} when assuming free transition
$y_{0.0125c}$	Upper-surface ordinate at 0.0125 chord
α	Angle of attack
ν	Kinematic viscosity
ρ	Density
$\theta_{0.020C}$	Angle of tangent to the upper surface at 0.020 chord

1 Introduction

Continuous operation in stalled conditions is unique for wind turbines compared to, e.g., helicopter rotors. Research in this field has revealed new details about the mechanisms of massive flow separation on a rotating wing. Three-dimensional and rotational effects (Milborrow, 1985, Rasmussen et al., 1988 and Madsen and Rasmussen, 1988) and dynamic stall (McCroskey, 1981) are important phenomena with strong influence on the maximum power and on the dynamic loads. Another important phenomenon is 'double stall'. The term 'double stall' originates from observations made early in the development of the stall-regulated turbines. Plots of power against wind speed showed two or more distinct power levels at high wind speeds. Each level could exist in periods ranging from minutes to hours. Likewise, the measurements of the blade root bending moments showed the distinct levels.

Double stall is undesirable for several reasons. It causes uncertainty in the estimation of the annual energy production and on the maximum loads on the turbine. More seriously, stall induced vibrations may be influenced by the quite different flow conditions and corresponding dynamic airfoil forces, which are related to double stall.

The objectives of the present work are first to describe different observations of double stall in full-scale rotor measurements and wind tunnel experiments. Next, possible causes of double stall are discussed. One of these causes, which is laminar separation bubbles at the leading edge of the airfoil, is described in detail based on the available literature on stall and based on detailed CFD calculations.

2 Experimental observations

Double stall has been observed on full-scale rotors and on airfoils in wind tunnel experiments. In the following section some of these observations will be described to verify the existence of double stall and to show that double stall originates from different distinct lift levels on the blades.

2.1 Rotors

Although observations of distinct different maximum power levels were made in the mid-eighties, no measurements relating to this specific subject seem to have been published from that period. Measurements on Danwin 23 180 kW turbines in the Alta Mesa wind farm in California (Pedersen et al., 1991) show two distinct stall levels in the rotor power as well as in the blade loads. The difference in level of the edgewise-bending moment is about 30%. The blades are based on the NACA 63-2nn series.

Other measurements by Bonus (1997) on a 600kW wind turbine give the electrical power as a function of wind speed at nacelle height as shown in Figure 2.1. The data are in the form of 10 min. average values for a period of one day. A drop in power output of about 150 kW, corresponding to 25%, is seen for a period of about one hour, after which the power regains its normal value. The loss of power occurred at a wind speed of about 16 m/s, which corresponds to a geometric angle of attack of approximately $\alpha \approx 16°$ and a Reynolds

number $Re \approx 2.6 \times 10^6$ at 0.9R for the particular blades. NACA 63-4nn series are used on the outer part of these blades, with NACA 63-415 at the tip, gradually changing to NACA 63-418 at 0.6R.

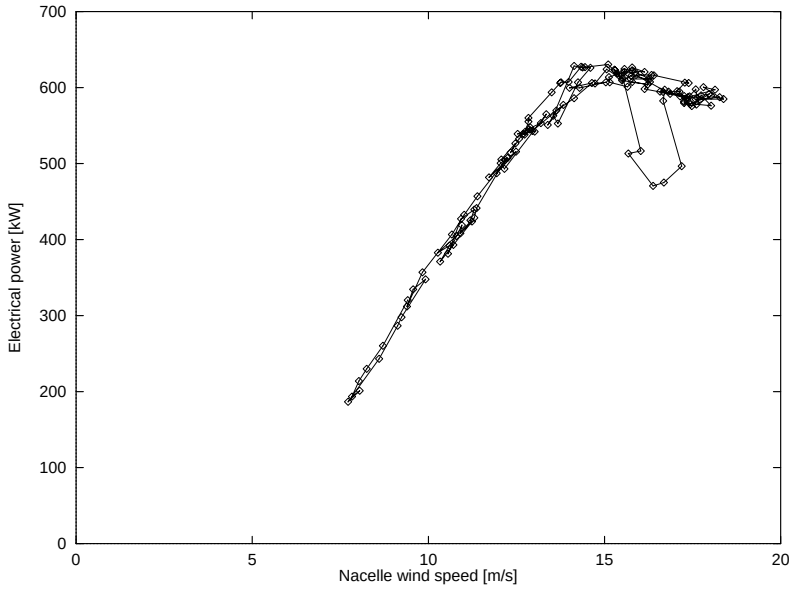

Figure 2.1. Measured electrical power for a 600 kW turbine. 10 minutes average values, Re=2.0-2.7x10^6, Bonus (1997).

2.2 Blade section on rotor

As part of the Risø Horizontal-Axis Wind Turbine (HAWT) experiments (Madsen, 1991), instantaneous local airfoil data were measured on a rotating LM 8.5 m blade at 0.68R. The blade is based on the NACA 63-2nn series with NACA 63-212 at the tip and gradually changing to NACA 63-218 at 0.5R and NACA 63-224 near the blade root. At 0.68R, the relative thickness ratio is 15.7%. The measured quantities versus angle of attack are the coefficients, $C_N=F_N/(qA)$ and $C_T=F_T/(qA)$, where F_N and F_T are the forces in the normal and tangential direction relative to the blade chord, respectively, q is the dynamic pressure and A is the area of the investigated blade segment. Such data are shown in Figure 2.2 from a 20 sec. time sequence (scan rate 25 Hz). Two preferred levels for the normal force coefficient, C_N, of approximately 1.5 and 1.3, can be identified with several shifts in between. To verify that the shifts between the two levels are double stall the number of samples are plotted versus C_N, reflecting double stall for α between 16° and 17°, Figure 2.3. The two preferred C_N levels are reflected in the peaks in Figure 2.3 for $C_N \approx 1.3$ and $C_N \approx 1.5$. The samples correspond to wind speeds around 10 to 11 m/s, assuming α to be geometrical, and $Re \approx 1.7 \times 10^6$. The two levels for C_T are less pronounced.

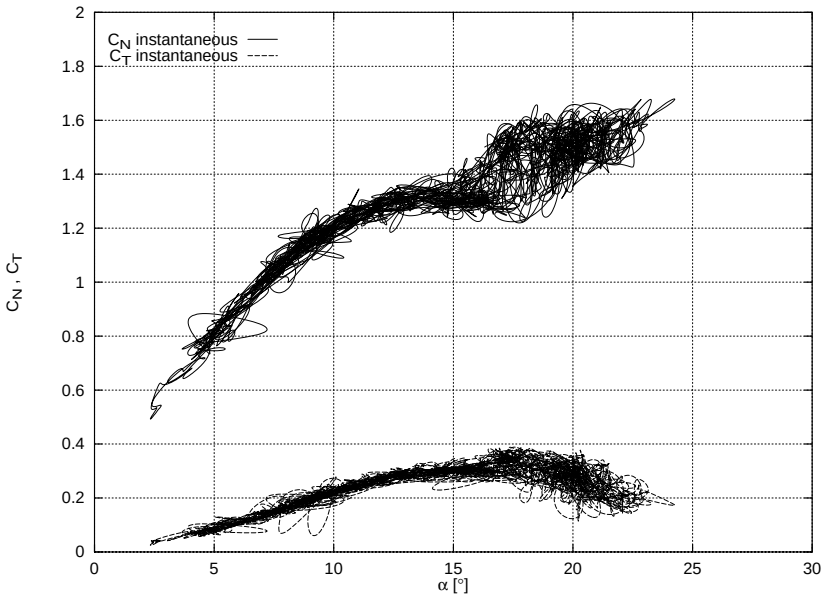

Figure 2.2. Measurement of instantaneous C_N and C_T on a full-scale rotating blade, Re≈1.7x10^6, Madsen (1991).

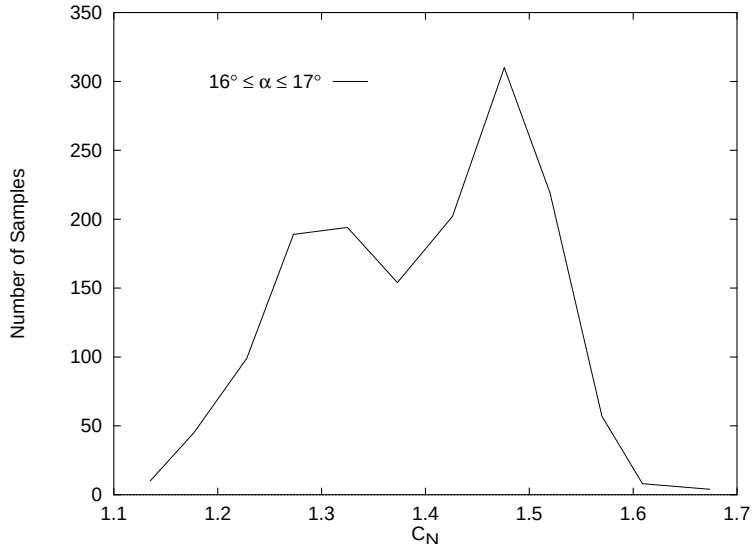

Figure 2.3. Number of samples versus C_N on a full-scale rotating blade, Re=1.7x10^6, corresponding to the C_N-values for α between 16° and 17° in Figure 2.2.

2.3 Blade section in wind tunnel

To investigate the stall behaviour without rotational effects, the blade used in the above experiment was also tested in a 4x4 m open-jet wind tunnel of cross section 7.5x7.5 m (Madsen and Rasmussen, 1993). The 4 m wide jet is centred on the blade section at 0.68*R*. The angle of attack, α, is increased in steps of 0.75° and remains constant for about 10 seconds on each step. Instantaneous measurements (scan rate 32 Hz) of C_N and C_T are shown in Figure 2.4. For α ranging from 16° to 28°, there is considerable scatter in the data and at least two C_N and C_T levels can be identified. A detailed analysis shows two preferred lev-

els in both C_N and C_T. The two levels for C_N are reflected in Figure 2.5, where two peaks appear for $C_N \approx 1.2$ and $C_N \approx 1.5$.

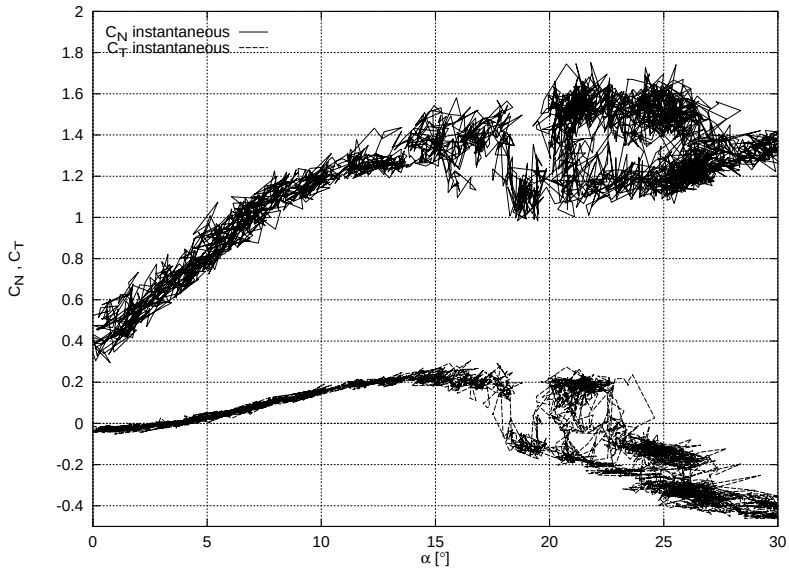

Figure 2.4. Measurements on a section of a full-scale blade in a 4x4 m open jet wind tunnel of cross section 7.5x7.5 m, Re=1.4x10^6, Madsen and Rasmussen (1993).

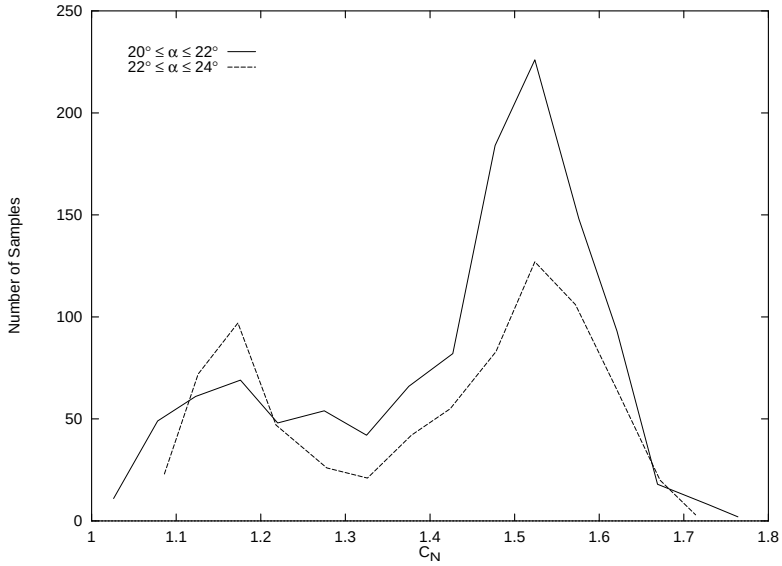

Figure 2.5. Number of samples versus C_N for α between 20-22 ° and 22-24 ° corresponding to the C_N-values Figure 2.4.

2.4 Non-tapered airfoil section in wind tunnel

To obtain more details about the different lift levels, Fuglsang et al. (1998a) conducted pressure measurements on a 1.9 m long non-tapered NACA 63-215 airfoil section in the open-jet wind tunnel. At constant α=15.3° (near $C_{L,max}$) C_L was measured as a function of time with a scan rate of 100 Hz, Figure 2.6. Three different levels of C_L can be identified: The low level around 1.0 (between 0 and 10 sec.), the intermediate level around 1.15 (between 130 and 180

sec.) and the high level at 1.27 (between 10 and 130 sec.). The shifts between the lift levels can thus be identified around 10 seconds and 130 seconds. In addition, tendencies to shifts from the high level to the intermediate level can be identified around 40 seconds and 70 seconds. Flow visualisation with tufts on the airfoil section showed the rather different flow patterns associated with the three levels.

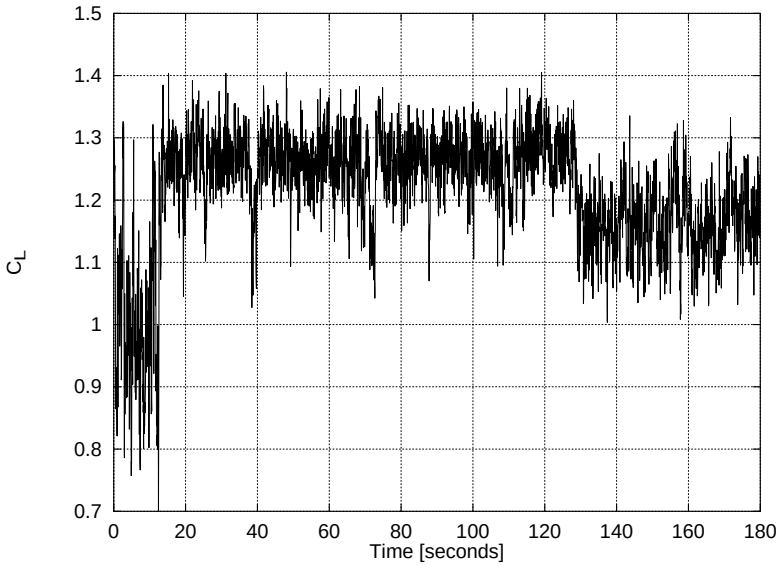

Figure 2.6. C_L versus time measured in a 2D test of a 1.9 m long blade section. α and average tunnel speed is constant, α=15.3 °, Re=1.3x10^6, Fuglsang et al. (1998a).

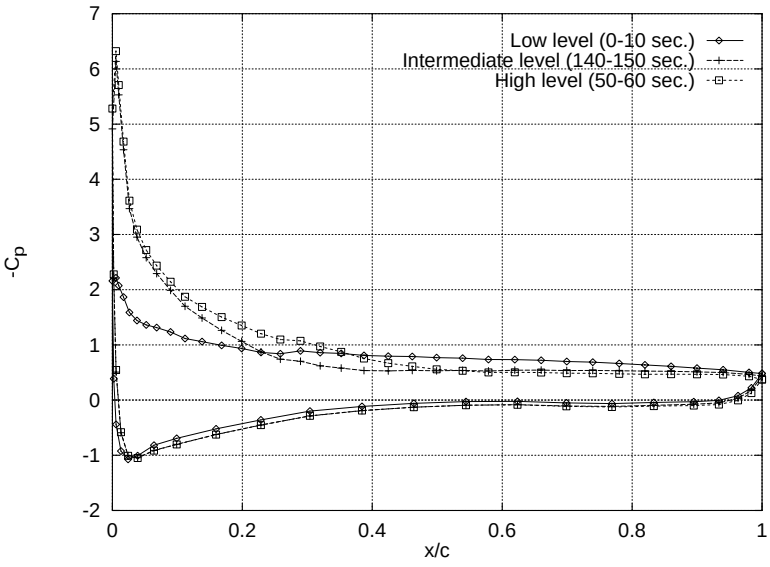

Figure 2.7. Time averaged C_p distributions corresponding to the three distinct C_L levels in Figure 2.6, Fuglsang et al. (1998a).

Finally, the three pressure distributions, C_p, corresponding to the different C_L levels are shown in Figure 2.7, where $C_p=(p-p_0)/q$, p is the pressure on the surface and p_0 is the pressure in the far field. The suction peak has almost disappeared in the pressure distribution for the low C_L level, whereas the difference between the two other pressure distributions mainly concerns the point of separation.

3 Explanations of double stall

Many hypotheses have been posed about the causes of double stall:

- changes in surface roughness, e.g., from rain or bugs,
- changes in turbulence intensity,
- changes in yaw error or wind shear,
- ice accumulation,
- salt crystal accumulation,
- stall hysteresis,
- laminar separation bubbles.

Due to the complex inflow situation in the free wind, it will often be difficult to reject one or more of the above causes, simply because all the necessary data are not monitored. This was the reason for carrying out the detailed wind tunnel measurements where the test conditions are better controlled and monitored.

The wind tunnel measurements on the full-scale blade Figure 2.4 and Figure 2.5, show that without actively changing the average test conditions, two different stall levels appear within a wide range of α (16°-28°) on this particular blade in three-dimensional flow. However, minor changes in the tunnel turbulence intensity can occur and the flexibility of the blade causes the effective incidence to fluctuate somewhat. The test results in Figure 2.6 confirm the above results for a rather different experimental set-up with approximately two-dimensional flow around the airfoil. Finally, the blade section measurements on the rotor, Figure 2.2 and Figure 2.3, show the same tendency as the wind tunnel measurements on the same blade, however, with C_N on the high level most of the time.

From the measurements described above we conclude that C_L can change between at least two different levels without any measured changes in external average conditions. This conclusion is in good agreement with observations described in the literature on stall for aeroplane airfoils. Here different distinct lift levels to identical inflow conditions are observed in the process of stall. Although the term ‘double stall’ is not used in the literature the observations described are very close to the observations made on double stall. In the following, some of the observations described in the literature on aeroplane airfoils will be referred.

3.1 Classification of stall types

In the investigation of stall in relation to aeroplanes, shifting lift levels to identical inflow conditions are observed in measurements on airfoil sections. Based on measurements Jones (1933,1934) describes a kind of race between leading-edge and trailing-edge stall for airfoils of moderate thickness and incidences near maximum lift. The process of double stall observed by Fuglsang et al. (1998a) can be described in the same way. Jones classifies stalling into three types, which McCullough and Gault (1951) describe in detail as

Trailing-edge stall (preceded by movement of the turbulent separation point forward from the trailing edge with increasing angle of attack). This appears typically on thick airfoils.

- Leading-edge stall (abrupt flow separation near the leading edge generally without subsequent reattachment). This appears typically on airfoils of moderate thickness.
- Thin-airfoil stall (preceded by flow separation at the leading edge with re-attachment at a point, which moves progressively rearward with increasing angle of attack). This appears typically on sharp-edge airfoils and thin rounded-leading-edge airfoils.

While the trailing-edge and thin-airfoil stall have a smooth development of the lift as a function of α, the leading-edge stall is characterised by a sudden loss of lift near maximum lift, Figure 3.1.

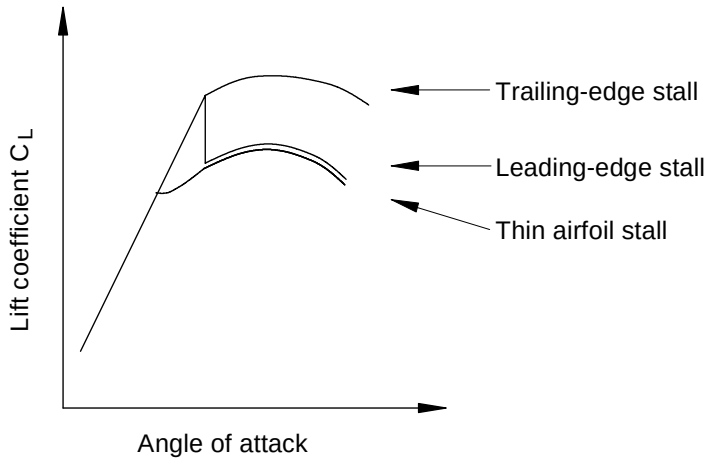

Figure 3.1. Sketch of the three stall types

Like Jones, also McCullough and Gault observed that there are some airfoil sections of intermediate thickness ratios which combine leading-edge stall and trailing-edge stall. Gault (1957) correlated approximately 150 NACA airfoils with Reynolds number and a single airfoil ordinate near the leading edge. He finds the combination of two different stall types on some airfoils. Apart from the three stall types, Gault thus includes a fourth type of stall in the correlation: A combined leading-edge and trailing-edge stall. This is shown in Figure 3.2, where the boundaries between the different types of stall are plotted as Reynolds number versus the upper-surface ordinate at 1.25% chord, $y_{0.0125c}$.

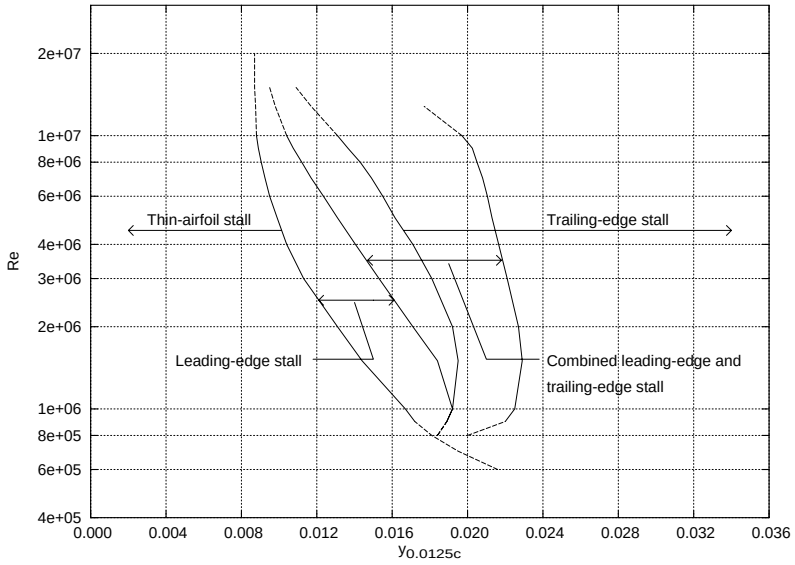

Figure 3.2. Stalling characteristics of NACA airfoil sections correlated with Re and $y_{0.0125c}$, Gault (1957).

As stated by Gault, the plotted boundaries are reasonably distinct. To emphasise the limitations and qualitative nature of the correlation he points out that the stall characteristics of the NACA 230nn-series are inconsistent with the general results of the analysis. For Reynolds numbers between 1×10^6 and 3×10^6 the correlation shows that combined leading-edge and trailing-edge stall will appear on the NACA 63-212, 63-215, 63-412 and 63-415 airfoil sections resulting in different lift levels.

3.2 The mechanisms of leading-edge stall

Jones (1934) and McCullough and Gault (1951) investigated the mechanisms underlying leading-edge stall. They find a laminar separation bubble at the leading edge before the abrupt leading-edge stall. Ward (1963) describes the laminar separation bubble as dependent on transition from laminar to turbulent flow. This transition occurs downstream of the laminar separation point. The resulting turbulent layer reattaches to the surface. Failure of the turbulent layer to reattach is known as 'bursting' and leading-edge stall will appear. As stated by Ward many explanations to the process of bursting have been suggested, but no agreement is found. Also Ward points out that increased turbulence will eventually move the transition point ahead of the laminar separation point and the bubble disappears.

An alternative to bubble bursting as the cause of leading-edge stall is reseparation. Ward suggests that turbulent separation can occur shortly downstream of reattachment. If the bubble is close to the leading edge, this flow pattern is often unstable. Thus, the turbulent separation point moves forwards and the bubble breaks down.

3.3 Parameters affecting stall

Gault's (1957) correlation, Figure 3.2, indicates that the airfoil shape and the Reynolds number have an effect on the type of stall. Furthermore as described by Hoerner and Borst (1975), the Reynolds number, the airfoil shape and the turbulence are important parameters affecting the maximum lift coefficient of

airfoils. They are factors, which determine the position of separation and thus maximum lift. Hoerner and Borst show that the maximum lift coefficient increases sharply at a certain Reynolds number except for very thin airfoils. This is the critical Reynolds number range where the boundary layer flow turns turbulent. This will cause the laminar-type separation from the suction side to disappear when the Reynolds number is increased. For a given nose-radius ratio (nose-radius relative to chord length) the critical Reynolds number decreases if the camber increases. In addition, for symmetrical airfoils, increasing the nose-radius ratio reduces the critical Reynolds number. Hoerner and Borst conclude that in the vicinity of $Re=1x10^6$ all sections with moderate thickness (between 8 and 12%) and small camber (between 0 and 2%) have a marked tendency of increased maximum lift coefficient as a function of Reynolds number. This is caused by an improved flow around the nose as the transition to turbulent flow moves further toward the leading edge. Furthermore, Hoerner and Borst conclude that all highly cambered and/or thicker airfoil sections (all sections with well-rounded noses) do not present difficulties to the flow around the leading edge. Using an airfoil of moderate thickness and low camber with a critical Reynolds number in the range of the operating Reynolds number could thus result in a change of stall type and thereby in a change of maximum lift. For comparison, the Reynolds number in the presented measurements varied between $1.3x10^6$ and $2.7x10^6$.

4 Numerical investigation

The literature on stall suggested to us that laminar separation and the associated strong influence on the stalling characteristics were the mechanisms responsible for double stall. A numerical investigation was carried out to study this hypothesis in details.

4.1 Method

Two-dimensional, steady state CFD calculations were carried out using the Navier Stokes solver EllipSys2D (Michelsen, 1992, Michelsen, 1994 and Sørensen, 1995). The flow near the leading edge was investigated on the NACA 63-215 and NACA 63-415 airfoils, which have 15% relative thickness and 1.0% and 2.1% camber, respectively. The influence of the airfoil shape was investigated by comparing the computations on the NACA airfoils to computations on the RISØ-1 airfoil. This airfoil has 14% relative thickness and 4.4% camber and is described by Madsen (1994), see Figure 4.1.

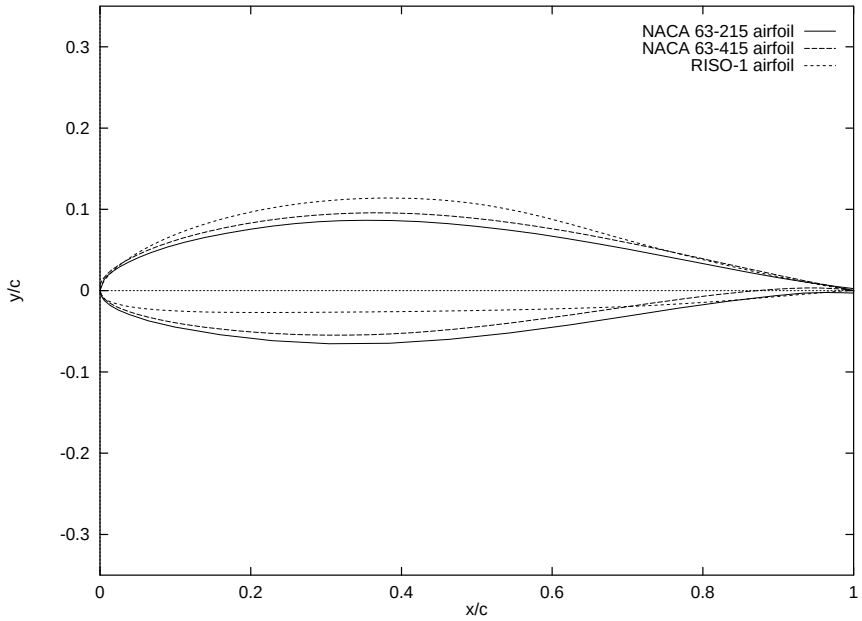

Figure 4.1. The NACA 63-215, NACA 63-415 and RISØ-1 airfoils.

The flow near the leading edge was investigated by analysing the transition from laminar to turbulent flow for different transition point positions in the leading edge region. Also free transition was investigated. The free transition point was found using the Michel criteria, Michel (1951).

All results were calculated with the EllipSys2D code using a three level grid sequence together with a SIMPLE algorithm (Patankar and Spalding, 1972). A second order upwind scheme was used for the convective terms in the momentum equations, and the SST k-ω turbulence model by Menter (1993) modelled the turbulence. An O-grid consisting of 288x72 cells was generated for each airfoil.

4.2 Results

NACA 63-215

The computed lift curve for NACA 63-215 is shown in Figure 4.2 for fully turbulent and transitional flow, respectively. For α beyond 11°, C_L for the transitional flow was lower than C_L for fully turbulent flow and for α=17° C_L was decreased 28%. The decrease in C_L for high α was caused by the generation of a laminar separation bubble. The bubble was generated at α=8° and existed until α=17°, where the suction side flow suddenly detached and leading-edge stall appeared. Figure 4.3 shows the length and height of the laminar separation bubble and in addition the position of the transition point. The transitional C_L was in good agreement with the experimental data by Fuglsang et al. (1998a).

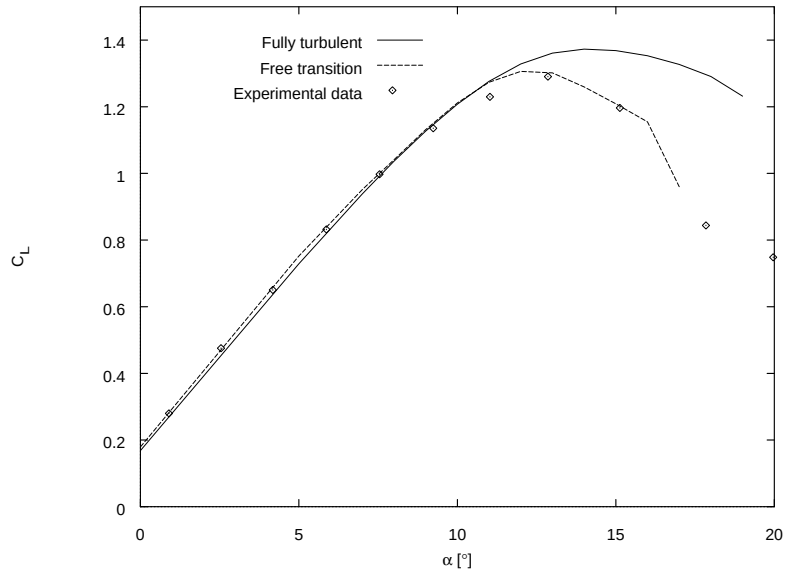

Figure 4.2. C_L versus α for Re=1.15x10^6, with and without transition, NACA 63-215. Experimental C_L curve measured by Fuglsang et al. (1998a).

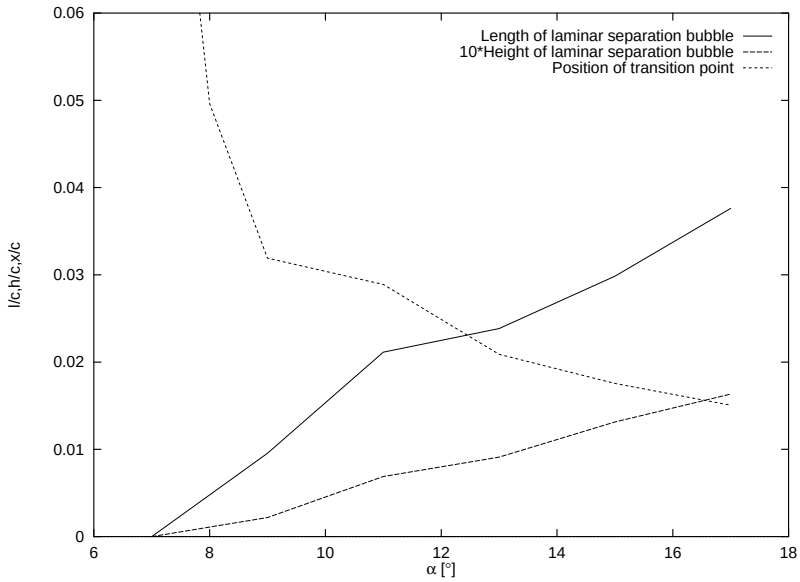

Figure 4.3. Length and height of the laminar separation bubble and the position of the transition point versus α, Re=1.15x10^6, NACA 63-215.

Further calculations were carried out near $C_{L,max}$ for α=15° to investigate the influence of the transition point location (x_{tr}) on the laminar separation bubble and thereby on the lift.

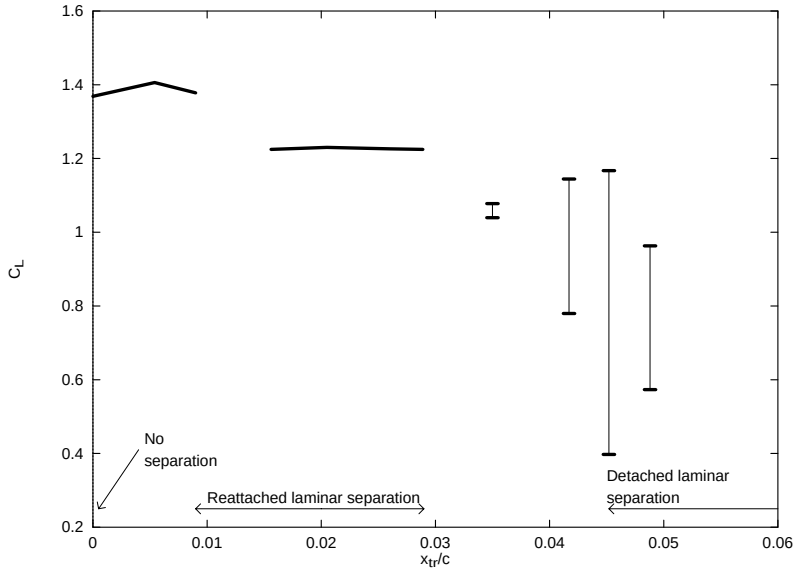

Figure 4.4. C_L versus transition point location (x_{tr}/c). α=15 °, Re=1.15x10^6, NACA 63-215.

Figure 4.4 shows how the lift level was affected by the position of the transition from laminar to turbulent flow in the boundary layer. Three different lift levels appeared when the transition point was fixed at different chordwise positions near the leading edge:

- A high level where the transition point was in the interval from 0 to 0.01*c*,
- An intermediate level where the transition point was between 0.01*c* to 0.03*c* (a laminar separation bubble followed by reattachment was observed as shown by the streamlines around the nose in Figure 4.6),
- A low level where the transition point was downstream of 0.03*c* (a laminar separation followed by severe fluctuations, which was leading edge stall).

A calculation using free transition showed that the transition point was fluctuating in the interval from 0.011*c* to 0.029*c*. It was noted that the maximum position of the fluctuating transition point for the free transition ($x_{tr,max}$=0.029*c*) was close to the fixed transition point, which caused leading-edge stall ($x_{tr,stall}$=0.03*c*). This indicated that a small disturbance could move the free transition point downstream and cause a shift to leading-edge stall.

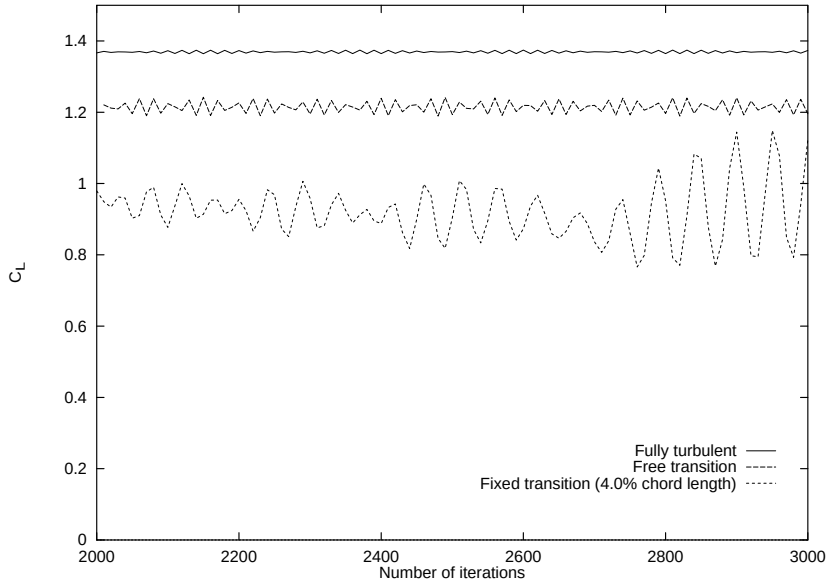

Figure 4.5. C_L versus number of iteration for three different cases: Fully turbulent flow, free transitional flow and flow assuming fixed transition at 0.04c. $Re=1.15x10^6$, $\alpha=15°$, NACA 63-215.

Although the flow became unsteady as the transition point moved downstream, the steady-state calculations revealed a qualitative picture of the mechanisms. Figure 4.5 shows C_L versus iteration number in three typical cases. It is seen that C_L was fluctuating in the calculations, where fully turbulent and free transitional flows were assumed. Nevertheless, they were averaged and thereby interpreted as steady state. This was in contrast to the calculation assuming fixed transition at 0.04*c* where severe fluctuations were observed.

An example of a laminar separation bubble is seen in Figure 4.6 where free transition was assumed. Pressure distributions are shown in Figure 4.7, for transition at the leading edge (fully turbulent), free transition and fixed transition at 0.05*c*.

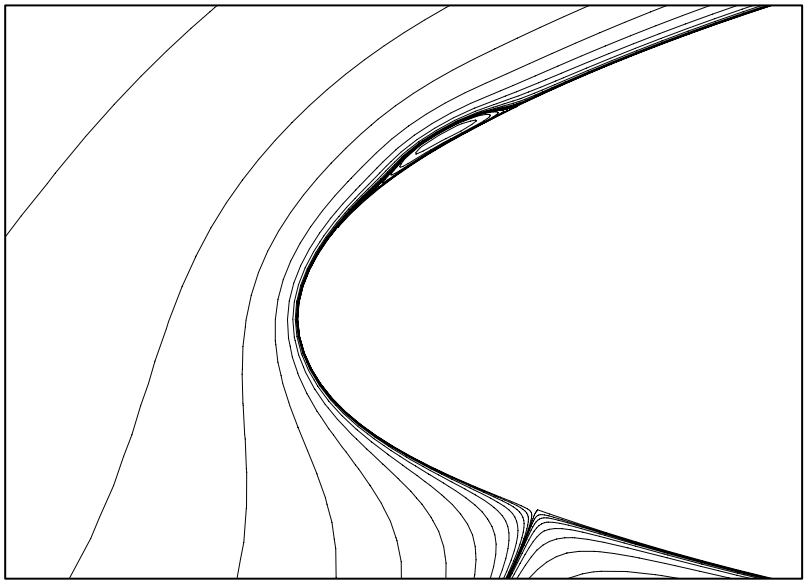

Figure 4.6. Streamlines around the NACA 63-215 for reattached laminar separation, $\alpha=15°$, $Re=1.15x10^6$ and assuming free transition.

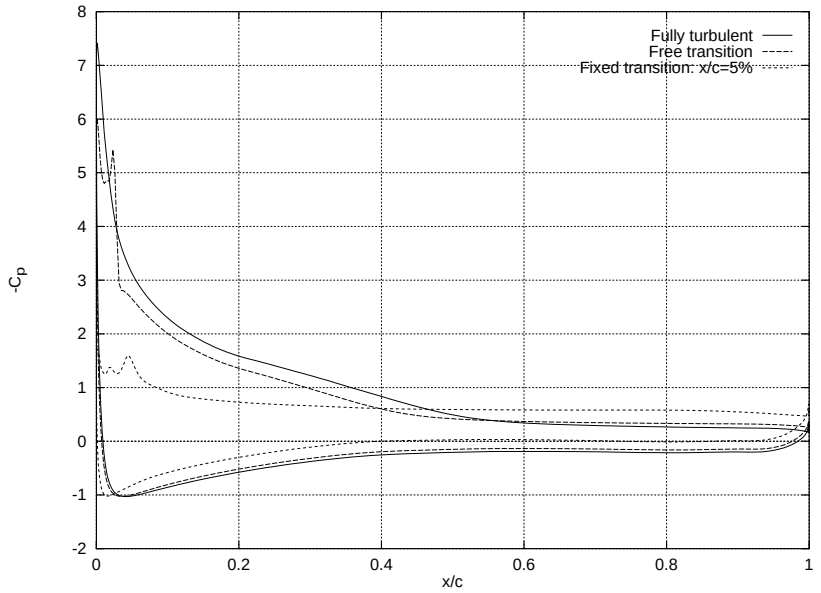

Figure 4.7. C_p distributions for three different flow modes, Re=1.15x10^6, α=15°, NACA 63-215.

According to Hoerner and Borst (1975) the $C_{L,max}$ level depends on the Reynolds number. CFD computations showed that for fixed α=15° C_L was increased with Reynolds number for fully turbulent flow as well as for transitional flow, as shown in Figure 4.8. It was noted that C_L fluctuated significantly for the free transitional flow until $Re \approx 5x10^5$. These fluctuations originated from leading-edge stall. Modern wind turbines operate in the Reynolds number range from 2x10^6 and 4x10^6 and in this interval, there was a steep increase in C_L for free transitional flow. This increase originated from a decrease in the laminar separation bubble, as shown in Figure 4.9, because the laminar separation bubble exists at the leading edge, where also the suction peak exists. The decrease in the bubble results in an increase of the suction peak and thereby in an increase in C_L.

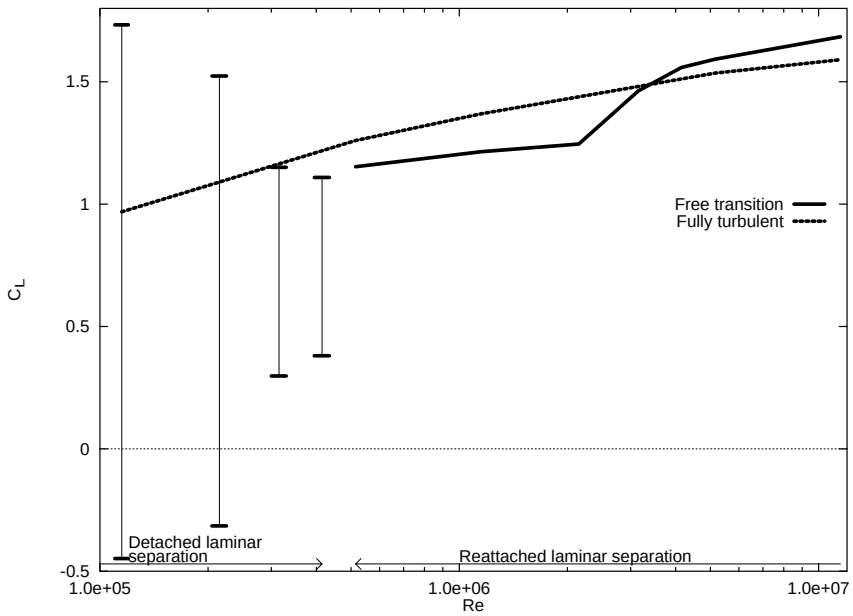

Figure 4.8. C_L versus Reynolds number, α=15°, NACA 63-215.

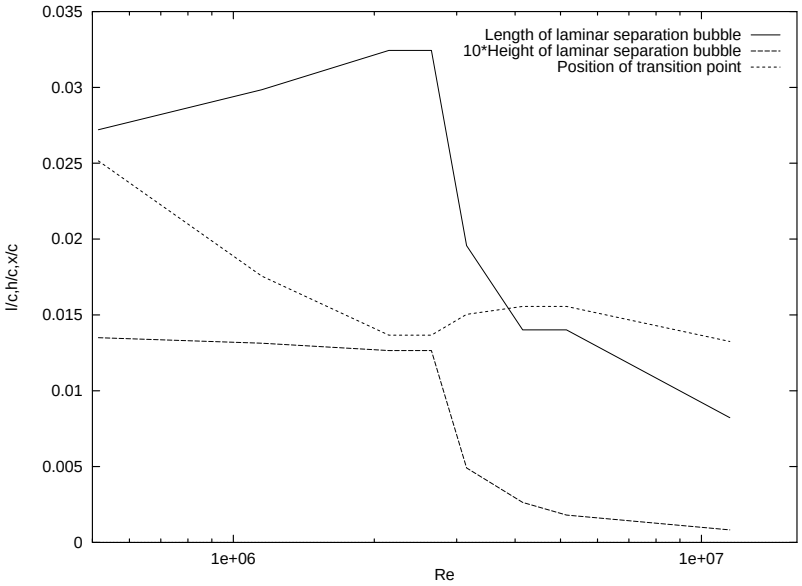

Figure 4.9. Length and height of the laminar separation bubble and the position of the transition point versus Reynolds number, α=15°, NACA 63-215.

NACA 63-415

Computations have also been carried out for the NACA 63-415 airfoil, which is used on many Danish wind turbines. The computed lift curve is shown in Figure 4.10 for fully turbulent and transitional flow, respectively. As it was the case for the NACA 63-215 C_L for the transitional flow was lower than C_L for fully turbulent flow for α beyond 11°. For α=17° C_L was decreased 19%, slightly less than the NACA 63-215 airfoil. Also in this case the decrease in C_L for high α was caused by the generation of a laminar separation bubble. This bubble was generated at α=8° and existed until α=17°, where the suction side flow suddenly detached and leading-edge stall appeared. Figure 4.11 shows the length and height of the laminar separation bubble and in addition the position of the transition point.

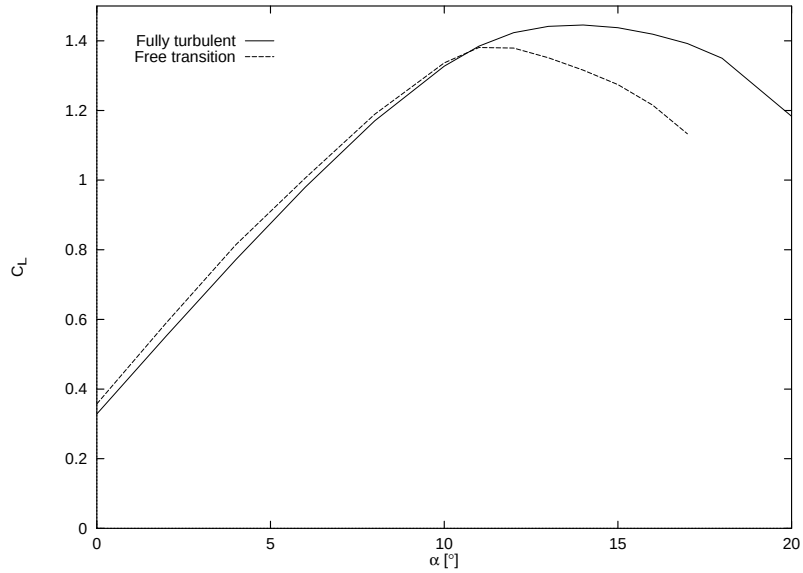

Figure 4.10. C_L versus α for Re=1.15x10^6, with and without transition, NACA 63-415.

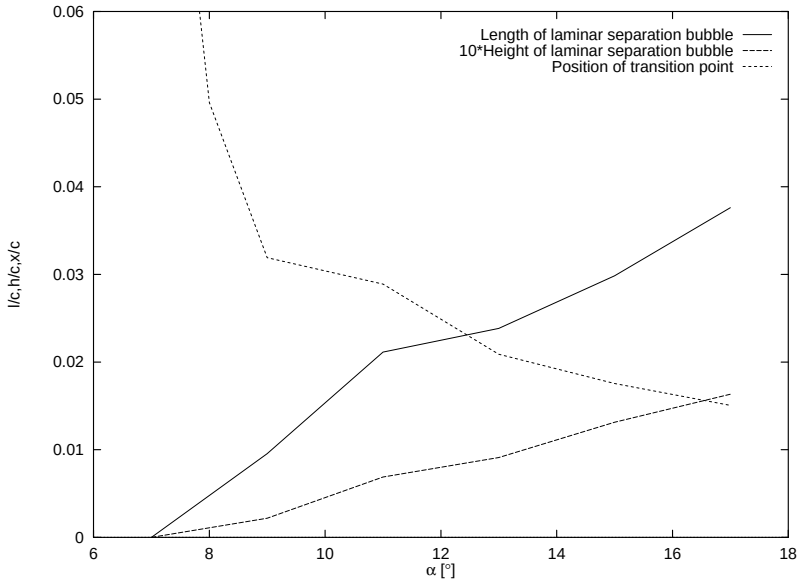

Figure 4.11. Length and height of the laminar separation bubble and the position of the transition point versus α, Re=1.15x10^6, NACA 63-415.

Calculations carried out near $C_{L,max}$ for α=15° to investigate the influence of the transition point location (x_{tr}) on C_L showed the same picture as was observed for the NACA 63-215 airfoil, Figure 4.12.

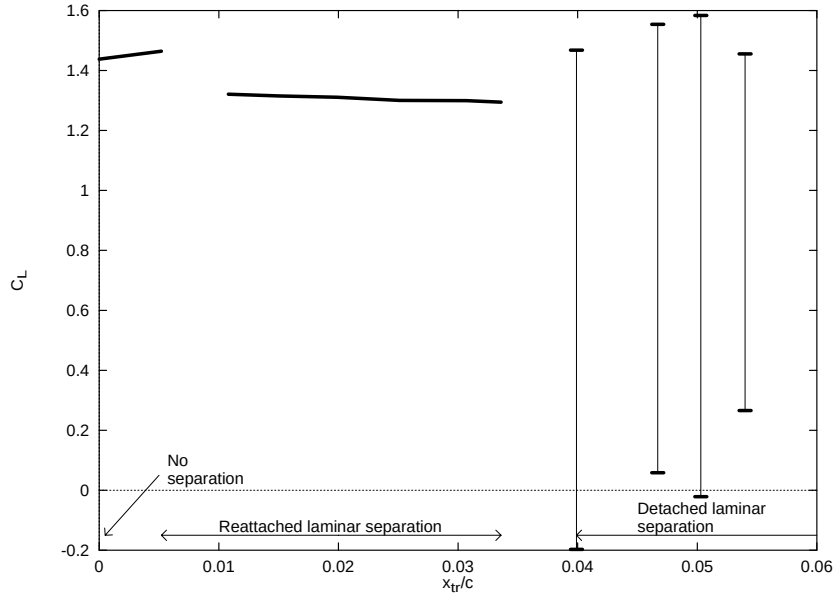

Figure 4.12. C_L versus transition point location (x_{tr}/c). α=15°, Re=1.15x10^6, NACA 63-415.

With the transition point fixed at different chordwise positions near the leading edge the calculations resulted in three different lift levels:

- A high level where the transition point was in the interval from 0 to 0.005*c*,
- An intermediate level where the transition point was between 0.005*c* to 0.035*c* (a laminar separation bubble followed by reattachment was observed),
- A low level where the transition point was downstream of 0.035*c* (a laminar separation followed by severe fluctuations, which was leading edge stall).

A calculation with free transition showed that the transition point was fluctuating in the interval from 0.007c to 0.031c. As for the NACA 63-215 airfoil the maximum position of the fluctuating free transition point ($x_{tr,max}$=0.031c) was close to the fixed transition point, which caused leading-edge stall ($x_{tr,stall}$=0.035c). A small disturbance could move the free transition point downstream and thus affect a shift to leading-edge stall as in the case of the NACA 63-215 airfoil.

Also the C_L dependence of Reynolds number showed the same picture as for the NACA 63-215 airfoil. Figure 4.13 shows for fixed α=15° an increasing C_L as the Reynolds number increases for fully turbulent flow as well as for transitional flow. For the transitional flow leading-edge stall existed until $Re \approx 4 \times 10^5$. A steep increase in C_L for the free transitional flow was observed in the Reynolds number range between 2×10^6 and 3×10^6. This increase originated from a decrease in the laminar separation bubble, Figure 4.14, as it was the case for the NACA 63-215 airfoil.

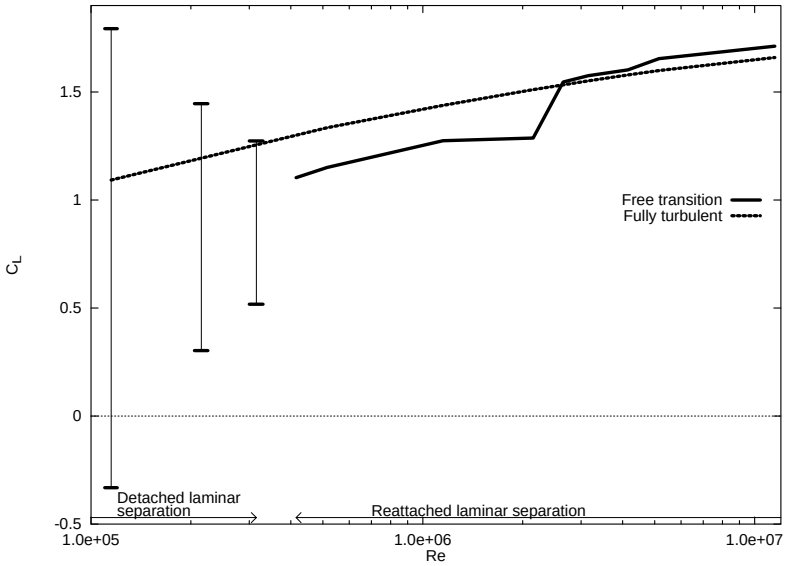

Figure 4.13. C_L versus Reynolds number, α=15°, NACA 63-415.

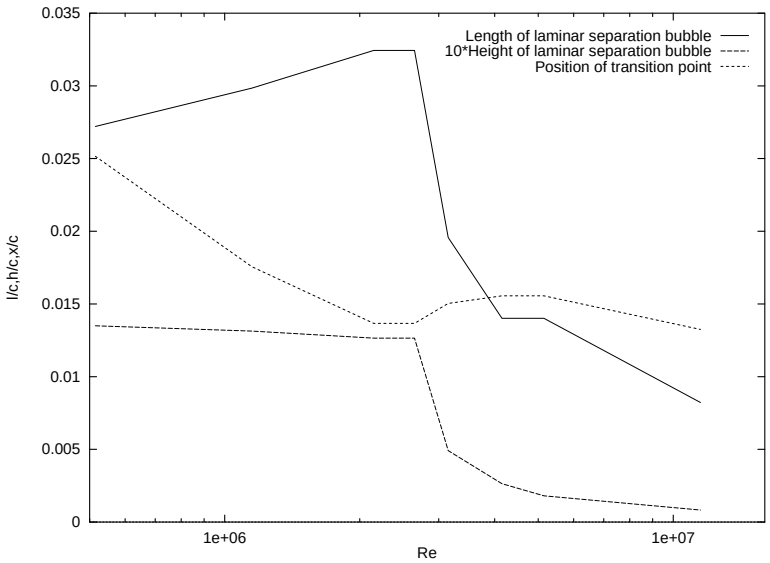

Figure 4.14. Length and height of the laminar separation bubble and the position of the transition point versus Reynolds number, α=15°, NACA 63-415.

The CFD computations on the NACA 63-415 showed that the characteristics of this airfoil were the same as for the NACA 63-215 airfoil, concerning the existence of a laminar separation bubble.

RISØ-1

To investigate the influence of the airfoil shape on the generation of a laminar separation bubble, computations were carried out for the RISØ-1 airfoil. This airfoil shape is different from the NACA airfoils, Figure 4.1.

The resulting C_L curve is shown in Figure 4.15. Free transition computations increased C_L relative to fully turbulent computations for α less than 16°. A laminar separation bubble near the leading edge was generated in the transitional case as it was the case for the NACA airfoils, but not until α beyond 14°. This bubble caused C_L to decrease slightly relative to the fully turbulent calculation for α beyond 16°. For α=18°, C_L for the transitional flow was decreased only 2.6%. This small difference was due to the airfoil geometry and especially the nose geometry, which had a strong influence on the position of the transition point. Figure 4.16 shows the size of the laminar separation bubble and the position of the transition point. The computed transitional C_L was in good agreement with the experimental data by Fuglsang et al. (1998b), however C_L was slightly overestimated in stall.

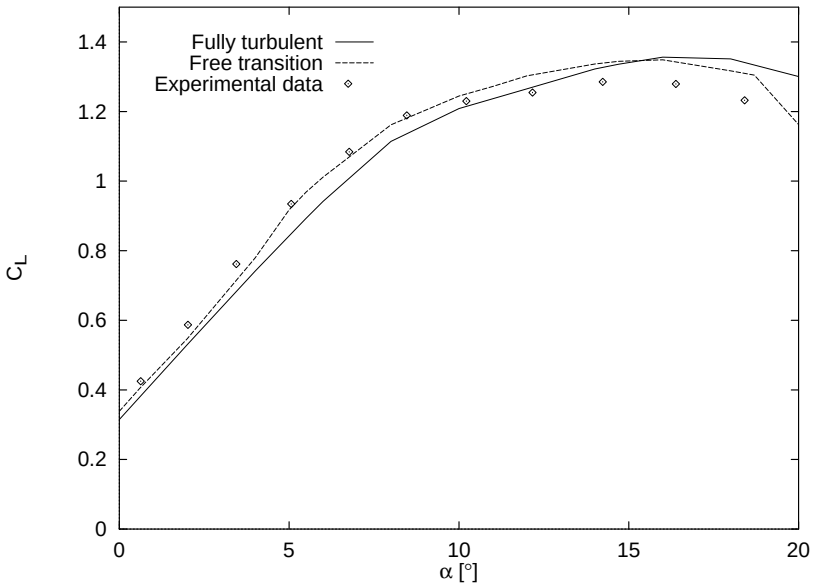

Figure 4.15. C_L versus α for Re=1.5x10^6, with and without transition. Experimental C_L curve measured by Fuglsang et al. (1998b), RISØ-1.

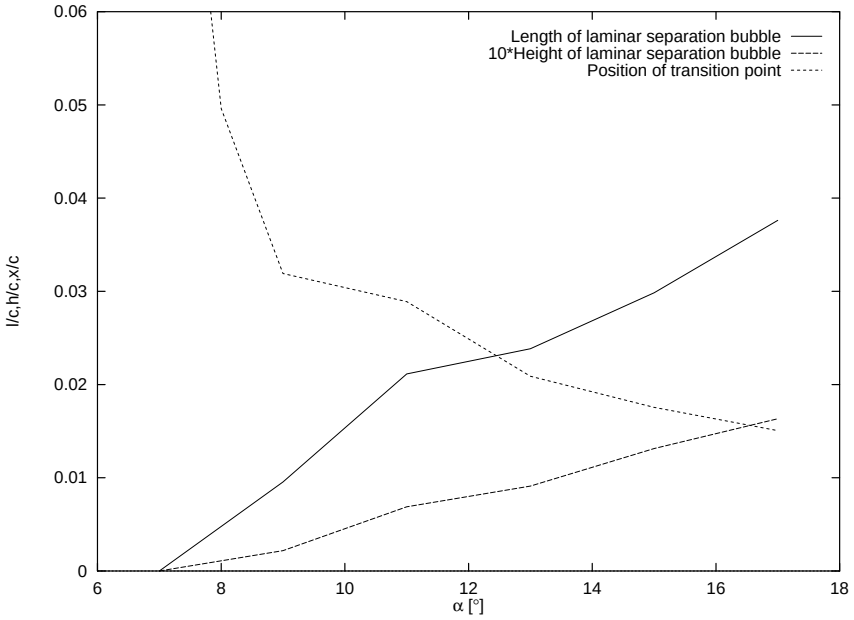

Figure 4.16. Length and height of the laminar separation bubble and the position of the transition point versus α, Re=1.5x10^6, RISØ-1.

Calculations were carried out to investigate the influence of x_{tr} on the laminar separation bubble and thereby on C_L. This was done near $C_{L,max}$ for α=18° because the stall behaviour around $C_{L,max}$ was of interest for comparison to the NACA airfoils. The point of transition, x_{tr}, was moved downstream until it passed 0.06c where the laminar separation bubble was detached. At this condition, the laminar separation was actually generated below 0.005c. This calculation resulted in a continuously and slightly decreasing C_L level, as shown in Figure 4.17. A calculation using free transition showed that the transition point was fluctuating in the range from 0.004c to 0.013c. Here it was noted that the maximum position of the transition point for free transition, $x_{tr,max}$=0.013c, was far from the minimum position of the transition point causing leading-edge stall, $x_{tr,stall}$=0.06c.

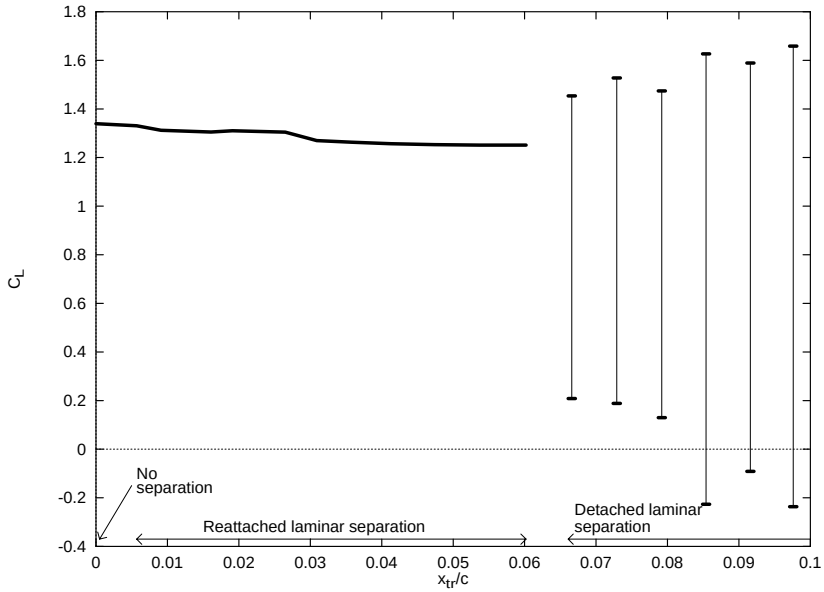

Figure 4.17. C_L versus transition point location (x_{tr}/c), Re=1.5x10^6, α=18°, RISØ-1.

Comparing the RISØ-1 airfoil to the NACA airfoils, the C_L dependence of Reynolds number showed another picture. Figure 4.18 shows for fixed α=18° an increasing C_L as the Reynolds number increases for fully turbulent flow as well as for transitional flow. For the transitional flow leading-edge stall only existed until $Re \approx 2 \times 10^5$. This was below $Re \approx 4 \times 10^5$, where leading-edge stall was observed on the NACA 63-415 airfoil. In contrast to the NACA airfoils no steep increase in C_L was observed for any Reynolds numbers, even though a laminar separation bubble existed in all Reynolds number ranges beyond $Re = 2 \times 10^5$, Figure 4.19.

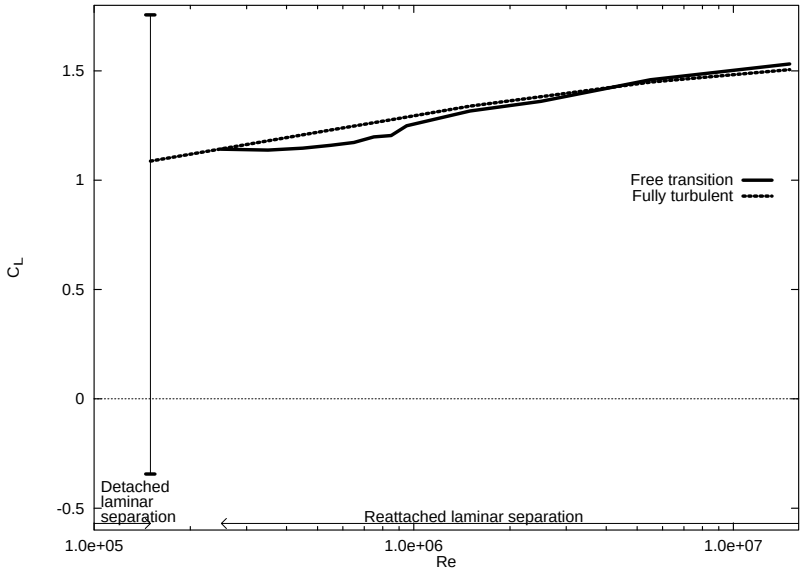

Figure 4.18. C_L versus Reynolds number, α=18°, RISØ-1.

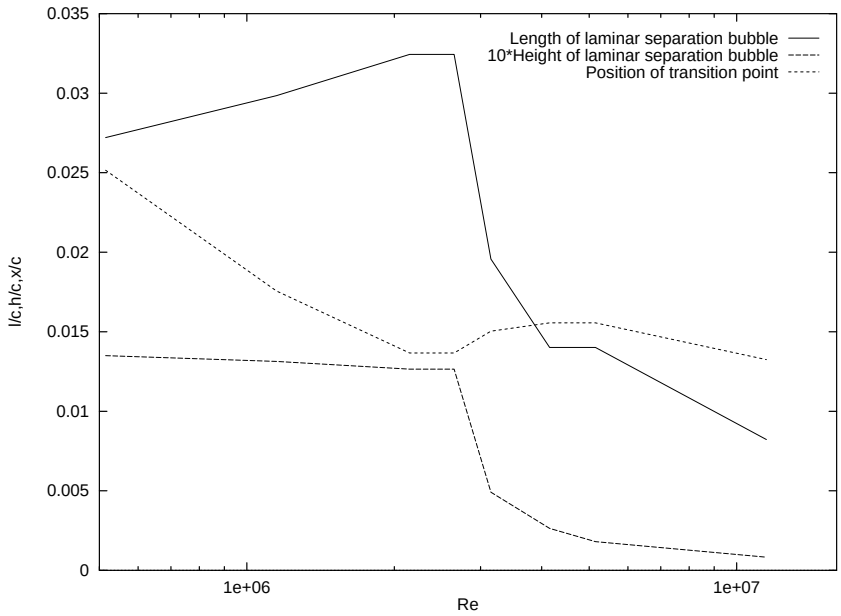

Figure 4.19. Length and height of the laminar separation bubble and the position of the transition point versus Reynolds number, α=18°, RISØ-1.

Thus, the RISØ-1 airfoil behaved quite different from the NACA airfoils, concerning the existence of a laminar separation bubble.

Comparison of the investigated airfoil sections

For both the NACA airfoils and the RISØ-1 airfoil, a laminar separation bubble was predicted when free transition was assumed. The bubble appeared for α >8° for the NACA airfoils, but not until α >14° for the RISØ-1 airfoil. This bubble caused a drop of 28% and 19% on C_L for transitional flow on the NACA airfoils for α=17° in contrast to the RISØ-1 airfoil, where the drop was only 2.6% for α=18°. This small drop was due to the nose geometry. The difference in geometry between the RISØ-1 airfoil and the NACA airfoils was that the RISØ-1 airfoil had a smaller nose radius and a steeper slope of the upper surface near the leading edge. Thus, the transition to turbulent flow appeared closer to the leading edge on the RISØ-1 airfoil than on the NACA airfoils. This difference in the position of transition could have a strong influence on the suction peak and thus an influence on the lift level.

Calculations on the NACA 63-215 airfoil revealed the existence of a laminar separation bubble if x_{tr} was fixed until $x_{tr,stall}$ =0.03c. Using free transition we found $x_{tr,max}$=0.029. Thus $x_{tr,max}$ was very close to $x_{tr,stall}$. The free transition bubble could then burst, since leading-edge stall could appear if x_{tr} was slightly beyond $x_{tr,max}$. This mechanism was also present for the NACA 63-415 airfoil. For the RISØ-1 airfoil the laminar separation bubble existed for transition fixed until $x_{tr,stall}$=0.06c. Using free transition we found $x_{tr,max}$=0.013c, far from $x_{tr,stall}$=0.06c and the free transition bubble then seemed to be stable. An explanation of double stall could thus be that $x_{tr,max}$ is very close to $x_{tr,stall}$ on airfoils showing double stall. Other CFD calculations on NACA 64-215 and NACA 64-221 were in good agreement with this explanation.

5 Stall characteristics correlation

To investigate the influence from the airfoil shape on double stall, we reviewed the correlation by Gault (1957), Figure 3.2. In this correlation, the stalling characteristics of three out of approximately 150 airfoils were inconsistent with the general results of the analysis, namely the NACA 23012, 23015 and 23018. Gault suggests that the stall characteristics of these airfoils were possibly preceded by an extremely rapid forward progression of the position of turbulent boundary-layer separation (i.e., a trailing-edge type of stall). Thus, the stall characteristics would as such agree with the correlation. To verify that the airfoils showed trailing-edge stall, steady state CFD calculations were carried out on the NACA 23015 assuming free transition. This showed a movement of the trailing-edge separation from 99% chord length at α=16° to 70% chord length at α=17° and further to 31% chord length at α=18° resulting in leading-edge stall for α=18.5°. Fluctuations in α in the wind tunnel could thus result in a sudden leading-edge stall caused by a rapid movement of the trailing-edge separation toward the leading edge. This indicated that the NACA 230nn series agreed with the correlation.

However, investigating the stall characteristics of the RISØ-1 airfoil, where $y_{0.0125c}/c$=0.0199, showed that combined leading-edge and trailing-edge stall was expected using the correlation by Gault. This was inconsistent with the observations by Fuglsang et al. (1998b), who observe only trailing-edge stall.

To make the correlation work also for other airfoils than NACA airfoils, e.g., the RISØ-1 airfoil, another parameter was chosen as the correlating parameter instead of the upper-surface ordinate. It was assumed that the leading-edge stall depended on the acceleration of the flow at the leading edge. Thus, we carried out a correlation for the stalling characteristics with Reynolds number and the angle of the tangent to the upper-surface at a certain chord station. Figure 5.1 shows a close correlation for the NACA airfoils between $y_{0.0125c}/c$ and the tangent to the upper-surface at 0.02c, $\theta_{0.020c}$. Figure 5.2 defines $y_{0.0125c}$ and $\theta_{0.020c}$.

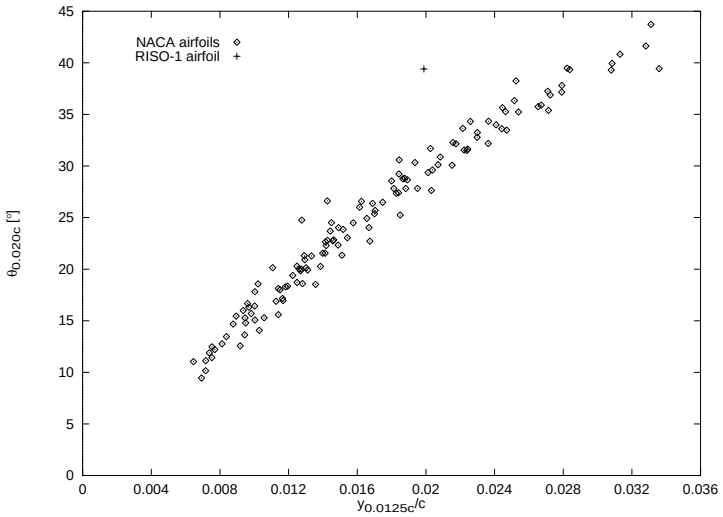

Figure 5.1. $\theta_{0.020c}$ as a function of $y_{0.0125c}/c$ for 138 NACA airfoils and the RISØ-1 airfoil.

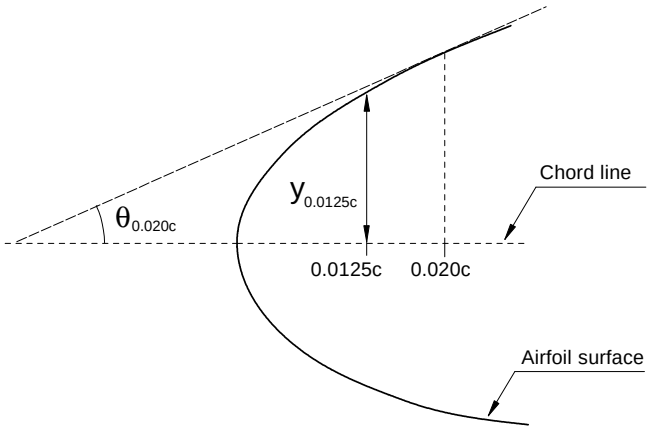

Figure 5.2. Definition of $y_{0.0125c}$ and $\theta_{0.020c}$.

This correlation using the 2.0% chord station was chosen because numerical investigations showed that detachment of the laminar flow at α=15° for the NACA 63-215 and 63-415 airfoil sections appeared when the transition point was at $x/c \approx 0.03$. Whether the flow detached or not depended on the development of the boundary layer for $x/c<0.03$. The correlation for different values of x/c showed that the best correlation between $y_{0.0125c}$ and $\theta_{0.020c}$ was found for $x/c>0.015$ and surface angles between x/c=0.015 and 0.03 should be chosen.

Altering the correlation by Gault (1957) from $y_{0.0125c}/c$ to $\theta_{0.020c}$ gives the picture in Figure 5.3. Since $\theta_{0.020c}$=39.4° for the RISØ-1 airfoil trailing-edge stall could be expected according to this correlation.

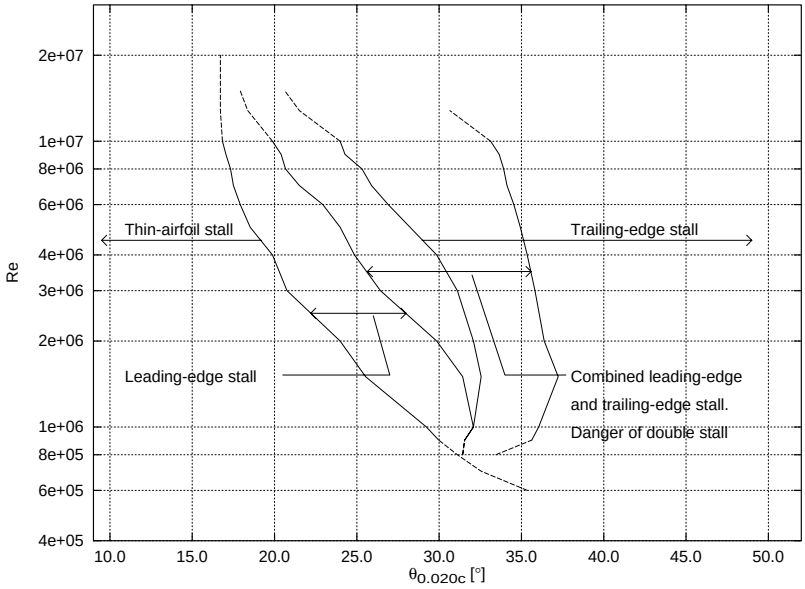

Figure 5.3. Stalling characteristics of airfoil sections correlated with Reynolds number and $\theta_{0.020c}$ *(based on data from Gault, 1957).*

The correlation was based on the boundaries limiting the stalling characteristics drawn by Gault, Figure 3.2. The angles, $\theta_{0.020c}$ as a function of $y_{0.0125c}/c$, shown in Figure 5.1 were averaged in the interval [$y_{0.0125c}/c$-0.0025 : $y_{0.0125c}/c$+0.0025] to get sufficiently smooth limits. The precision of this correlation relative to the correlation by Gault was typically $\theta_{0.020c}$±1.5°, with a maximum of $\theta_{0.020c}$±4.0°. In the present correlation, only the airfoils analysed by Gault were used, Appendix 1.

Since the stall characteristics depends on pressure gradients, transitional phenomena etc. at the nose, it is not believed that one parameter in the form of neither $y_{0.0125c}$ nor $\theta_{0.020c}$ can describe the stall characteristics of an airfoil. As emphasised by Gault (1957) this kind of correlation is of qualitative nature and can only give a picture of the parameters of the airfoil geometry affecting the stall characteristics.

6 Discussion

The numerical investigation of the NACA airfoil sections revealed the existence of a laminar separation bubble at the leading edge for α between 8° and 17° when assuming free transition. As stated by Ward (1963) the existence of a laminar separation bubble can lead to bubble bursting. This will cause leading-edge stall and thereby an abrupt loss of lift. Furthermore, calculations revealed three possible flow regimes in stall: The trailing-edge stall, the laminar separation bubble at the leading edge followed by trailing-edge stall, and the leading-edge stall. The distance between the free transition point and the transition point that would cause leading-edge stall controlled the three flow regimes. This resulted in three levels of C_L. Fuglsang et al. (1998a) describe measurements on a

NACA 63-215 airfoil section and also find three levels for C_L at α=15.3°. Comparing the measured pressure distributions in Figure 2. with predicted pressure distributions in Figure 4.7, good agreement was found.

Hoerner and Borst (1975) conclude that all highly cambered and/or thicker airfoil sections do not present difficulties to the flow around the leading edge. Since the RISØ-1 airfoil has 4.4% camber and the NACA 63-215 and NACA 63-415 airfoil have only 1.0% and 2.1% camber, respectively, the numerical investigations agreed with this conclusion. In addition, the measurements on the NACA 63-215 and the RISØ-1 airfoil section by Fuglsang et al. (1998a, 1998b) also support this conclusion. Comparing the NACA airfoils and the RISØ-1 airfoil, the RISØ-1 nose radius was smaller, and the slope of the upper-surface near the leading edge was steeper. The steep slope of the upper-surface could stabilise the flow and the small nose radius could cause transition close to the leading edge, far from the point of transition where leading-edge stall would appear, $x_{tr,stall}$. This could avoid bursting of the laminar separation bubble and thereby avoid double stall.

The wind tunnel experiments and the CFD calculations showed that double stall appeared near $C_{L,max}$. Relating these observations to the rotor measurements, good agreement was found. Thus, the loss of lift on the rotor observed by Bonus (1997) appears near $C_{L,max}$ (geometrically $\alpha \approx 16°$ at $0.9R$). In the measurements by Madsen (1991) double stall is also found near $C_{L,max}$. Gault (1957) show that double stall can appear on the airfoil sections NACA 63-212, NACA 63-215 and NACA 63-415. These airfoil sections are used on the outer part of the rotors showing double stall and it could be expected that these rotors sometimes show a loss of power.

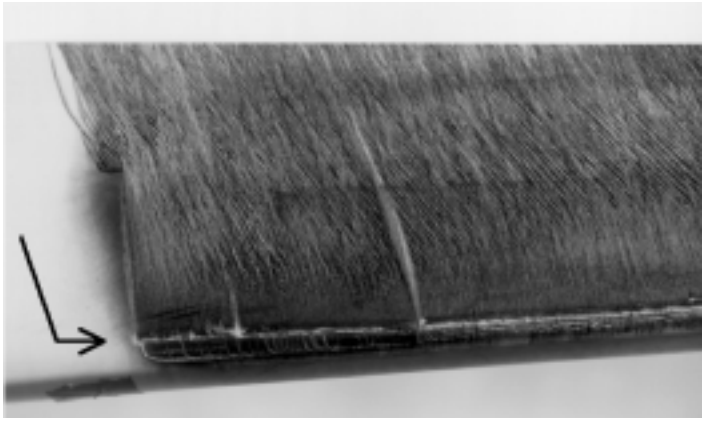

Figure 6.1. Oil flow visualisation on a rotating blade, $Re \approx 2.7 \times 10^6$. The arrow points out the trace of the laminar separation bubble, which is the white line at the leading edge. The flow is from bottom to top.

Oil flow visualisation on a rotating blade, Figure 6.1, indicates that the laminar separation bubble observed in two-dimensional flow also exists in three-dimensional, rotating flow. Figure 6.1 shows that during operation at high wind speeds, a laminar separation bubble was formed at the leading edge along the outer blade span. Milborrow (1985) concludes that radial flows sustain and enhance suction on the airfoil, delaying stall and enhancing lift. This means that the rotational effects will influence the flow, in particular around the bubble and in the separated regions. This may cause the flow to avoid leading-edge stall and instead have preference for higher lift levels during operation on a rotor compared to non-rotational flow as indicated by the measurements shown in Figure 2.2 and Figure 2.4.

Measurements, numerical investigations and the correlation by Gault (1957) showed that the stall characteristics depended strongly on the airfoil shape at the leading edge. A certain change of the geometry around the nose for airfoils showing double stall could remedy the double stall characteristics.

7 Conclusions

- A likely explanation of double stall was found from CFD calculations on the NACA 63-215 and NACA 63-415 airfoils. Three different lift levels were found depending on the location of the transition point near the leading edge. The generation of a laminar separation bubble at the leading edge of the airfoil near maximum lift and the bursting of this bubble could explain the sudden shift in lift levels.
- The investigation indicated that double stall can be predicted from CFD calculations. Computations on NACA 63-215, 63-415, 64-215, 64-221 and RISØ-1 airfoil indicated that bursting of the laminar separation bubble could be predicted. This was done by comparing the maximum position of transition using free transition with the minimum position of transition causing leading-edge stall using fixed transition. Bursting and thereby double stall could appear if these two positions were close to each other.
- The present investigation indicated that double stall can be avoided in design of new airfoils.

References

Bonus A/S, Denmark, Private communication with Peder Enevoldsen (1997).

Gault, D.E., 'A Correlation of Low-Speed, Airfoil-Section Stalling Characteristics With Reynolds Number and Airfoil Geometry', NACA Tech. Note 3963, (1957).

Fuglsang, P., Antoniou, I., Sørensen, N.N. and Madsen, H.A., 'Validation of a Wind Tunnel Testing Facility for Blade Surface Pressure Measurements', Risø-R-981(EN), Risø National Laboratory, Denmark (1998a).

Fuglsang, P., Antoniou, I., Bak, C. and Madsen, H.A., 'Wind Tunnel Tests of the RISØ-1 Airfoil', Risø-R-999(EN), Risø National Laboratory, Denmark (1998b).

Hoerner, S.F. and Borst, H.V., *Fluid-Dynamic Lift*, Hoerner Fluid Dynamics, Brick Town, 1975

Jones, B.M., 'An Experimental Study of the Stalling of Wings', R.&M. No. 1588, British A.R.C. (1933).

Jones, B.M., 'Stalling', Jour. Royal Aero. Soc., **38**, no. 285 (22d Wilbur Wright Memorial Lecture), 753-770 (1934).

Madsen, H.A., 'Aerodynamics of a Horizontal Axis Wind Turbine in Natural Conditions', Risø-M-2903, Risø National Laboratory, Denmark (1991).

Madsen, H.A., 'Design of a 20 kW - 12,6 m stall regulated rotor' (in Danish), Risø-I-809(DA), Risø National Laboratory, Denmark (1994).

Madsen, H.A. and Rasmussen, F., 'Derivation of Three Dimensional Airfoil Data on the Basis of Experiment and Theory', Proc. Windpower ´88, Honolulu, Hawaii (1988).

Madsen, H.A. and Rasmussen, F., 'Steady and Unsteady Wind Tunnel Measurements on a Blade Section', Proc. of the 7th IEA Symposium on the Aerodynamics of Wind Turbines, Lyngby, Copenhagen, Denmark (1993).

McCroskey, W.J., 'The Phenomenon of Dynamic Stall', NASA Tech. Memo. 81264 (1981).

McCullough, G.B. and Gault, D.E., 'Examples of Three Representative Types of Airfoil-Section Stall at Low Speed', NACA Tech. Note 2502, (1951).

Menter, F.R., 'Zonal Two Equation k-ω Turbulence Models for Aerodynamic Flows', AIAA-paper-93-2906 (1993).

Michel, R., 'Etude de la Transition sur les Profiles d'Aile; Establissement d'un Critére de Determination de Point de Transition et Calcul de la Trainee de Profile Incompressible', ONERA, Tech. Rep. 1/1578-A (1951).

Michelsen, J.A., 'Basis3D - a Platform for Development of Multiblock PDE Solvers', Technical Report AFM 92-05, Technical University of Denmark (1992).

Michelsen, J.A., 'Block Structured Multigrid Solution of 2D and 3D Elliptic PDE's', Technical Report AFM 94-06, Technical University of Denmark (1994).

Milborrow, D.J., 'Changes in aerofoil characteristics due to radial flow on rotating blades', Wind Energy Conversion 1985, Proc. of the 7th British Wind Energy Association Conference, Oxford 27-29 March 1985, Mech. Eng. Publications Ltd. (1985).

Patankar, S.V. and Spalding, D.B., 'A calculation Procedure for Heat, Mass and Momentum Transfer in Three-Dimensional Parabolic Flows', Int. J. Heat Mass Transfer, vol. 15, p. 1787 (1972a)

Patankar, S.V. and Spalding, D.B., 'A Computer Model for Three-Dimensional Flow in Furnaces', Proc. 14th Symp. (Int.) in Combustion, The Combustion Inst., p 605 (1972b)

Pedersen, T.F., Petersen, S.M., Thomsen, K., Madsen, P.H. and Højstrup, J., 'Loads for Wind Turbines in Inhomogeneous Terrain. Measurement Report', Risø-M-2922. Risø National Laboratory, Denmark (1991).

Rasmussen, F., Petersen, S.M., Larsen, G., Kretz, A. and Andersen, P.D., 'Investigations of Aerodynamics, Structural Dynamics and Fatigue on Danwin 180 kW', Risø-M-2727, Risø National Laboratory, Denmark (1988).

Sørensen, N.N., 'General Purpose Flow Solver Applied to Flow over Hills', Risø-R-827(EN), Risø National Laboratory, Denmark (1995).

Ward, J.W., 'The Behaviour and Effects of Laminar Separation Bubbles on Aerofoils in Incompressible Flow', Jour. Royal Aero. Soc., **67**, 783-790 (1963).

Appendix 1 Correlated data

For the correlation based on the correlation by Gault (1957) the data in Table 1 was used.

Table 1. Upper-surface ordinates at the 0.0125-chord station and the angle of the tangent to the upper-surface at 0.020-chord station ($y_{0.0125C}/c$[percent chord], $\theta_{0.020C}$[°]) for different airfoil sections and different relative thickness.

NACA airfoil series	Thickness ratio, percent chord								
	6	8	9	10	12	15	18	21	24
00XX	0.95, 15.28	1.26, 20.02	1.42, 22.29	1.58, 24.49	1.89, 28.66	2.37, 34.34	2.84, 39.34	3.31, 43.72	3.78, 47.54
24XX	1.11, 20.14	1.45, 24.51	1.62, 26.57	1.80, 28.55	2.16, 32.27	2.71, 37.25	3.28, 41.63	3.87, 45.41	4.47, 48.69
44XX	1.28, 24.75		1.84, 30.59		2.45, 35.65	3.08, 39.95	3.76, 43.68	4.47, 46.82	5.22, 49.52
230XX	1.42, 26.61		2.03, 31.70		2.67, 35.90	3.36, 39.44	4.09, 42.34	4.85, 44.76	5.66, 46.79
16-0XX	0.65, 11.04		0.97, 16.31		1.29, 21.31	1.61, 25.99	1.94, 30.33	2.26, 34.32	
63-0XX	0.77, 12.21		1.15, 18.00	1.27, 20.00	1.52, 23.85	1.88, 28.80	2.21, 33.65	2.52, 38.25	
63-2XX	0.89, 15.45		1.29, 20.91	1.43, 22.79	1.69, 26.38	2.08, 30.87	2.46, 35.27	2.82, 39.47	
63-4XX	1.02, 18.57		1.44, 23.69		1.87, 28.75	2.30, 32.78	2.72, 36.89	3.13, 40.83	
64-0XX	0.75, 11.43	1.00, 15.07	1.13, 16.89	1.25, 18.71	1.49, 22.33	1.84, 27.41	2.18, 32.16	2.51, 36.34	
64-2XX	0.88, 14.67	1.14, 18.12	1.27, 19.84	1.40, 21.54	1.66, 24.92	2.04, 29.61	2.41, 33.99	2.79, 37.81	
64-4XX	1.00, 17.81		1.41, 22.65		1.83, 27.35	2.24, 31.64	2.65, 35.75	3.08, 39.30	
65-0XX	0.72, 10.16	0.94, 13.63	1.06, 15.29	1.17, 16.95	1.39, 20.27	1.70, 25.36	2.01, 29.36	2.30, 33.24	
65-2XX	0.84, 13.46		1.19, 18.35	1.31, 19.92	1.54, 23.05	1.88, 27.82	2.22, 31.55	2.54, 35.23	
65-4XX	0.96, 16.66		1.33, 21.28	1.46, 22.75	1.70, 25.69	2.07, 30.12	2.44, 33.61	2.79, 37.16	
66-0XX	0.69, 9.45	0.92, 12.57	1.03, 14.08	1.14, 15.59	1.36, 18.53	1.67, 22.71	1.95, 27.83	2.24, 31.50	
66-2XX	0.81, 12.77		1.16, 17.16	1.28, 18.60	1.51, 21.35	1.85, 25.25	2.15, 30.07	2.47, 33.48	
66-4XX	0.94, 15.99		1.30, 20.13		1.67, 24.03	2.03, 27.63	2.36, 32.17	2.71, 35.39	
63A0XX	0.75, 12.47	1.00, 16.43		1.25, 20.29	1.49, 24.02	1.84, 29.23			
64A0XX	0.74, 11.88	0.98, 15.70		1.22, 19.39	1.46, 22.84	1.81, 27.82			
65A0XX	0.72, 11.12	0.95, 14.79		1.18, 18.29	1.41, 21.54	1.75, 26.49			

RISØ-1 airfoil: 1.99, 39.41

Bibliographic Data Sheet **Risø-R-1043(EN)**

Title and authors

Double Stall

Christian Bak, Helge Aagaard Madsen, Peter Fuglsang, Flemming Rasmussen

ISBN	ISSN
87-550-2379-7 87-550-2417-3 (Internet)	0106-2840

Department or group	Date
Wind Energy and Atmospheric Physics Department	June 98

Groups own reg. number(s)	Project/contract No(s)
1110-013-00	ENS 1363/97-0002

Pages	Tables	Illustrations	References
31	1	32	24

Abstract (max. 2000 characters)

The double stall phenomenon for airfoil flows is characterised by at least two distinct stall levels to identical inflow conditions. In this work, a likely explanation of double stall was found. Observations on full-scale rotors, in wind tunnel experiments and in computational fluid dynamic (CFD) calculations could show at least two different distinct lift levels to identical inflow conditions in stall. The CFD calculations revealed a generation of a little laminar separation bubble at the leading edge of the airfoil for incidences near maximum lift. The bursting of this bubble could explain the sudden shift in lift levels. This investigation indicated that bursting would appear if the maximum position of the free transition point was close to the minimum position of the transition point causing leading-edge stall. Thus, the investigation indicated that double stall could be predicted from CFD calculations and that double stall therefore could be avoided in design of new airfoils.

Descriptors INIS/EDB

AERODYNAMICS; AIRFOILS; TURBINE BLADES; STALL; LAMINAR FLOW; TURBULENT FLOW; TWO-DIMENSIONAL CALCULATIONS; WIND TUNNELS; VALIDATION; COMPUTATIONAL FLUID DYNAMICS

Available on request from Information Service Department, Risø National Laboratory,
(Afdelingen for Informationsservice, Forskningscenter Risø), P.O.Box 49, DK-4000 Roskilde, Denmark.
Telephone +45 46 77 40 04, Telefax +45 46 77 40 13